


 Cite this: *RSC Adv.*, 2022, **12**, 22893

Recurrent neural network (RNN) model accelerates the development of antibacterial metronidazole derivatives†

 Nannan Chen,[‡]^a Lijuan Yang,[‡]^{bc} Na Ding,^a Guiwen Li,^a Jiajing Cai,^a Xiaoli An,^b Zhijie Wang,^a Jie Qin^{*a} and Yuzhen Niu  ^{*a}

Metronidazole is a specific drug against trichomonas and anaerobic bacteria, and is widely used in the clinic. However, extensive clinical application is often accompanied by extensive side effects, so it is still of great significance to develop metronidazole derivatives with a new skeleton. Compared with other traditional receptor-based drug design methods, the computational model based on a neural network has higher accuracy and reliability. In this work, a Recurrent Neural Network (RNN) model is applied to the discovery of metronidazole drugs with a new skeleton. Firstly, the generation model based on a Gated Recurrent Unit (GRU) is trained to generate an effective Simplified Molecular-Input Line-Entry System (SMILES) string library with high precision. Then, transfer learning is introduced to fine-tune the GRU model, and many molecules with structures similar to known active drugs are generated. After cluster analysis of the structures of the new compounds, 20 small molecular compounds with metronidazole structures of all different categories were selected, of which 19 may not belong to any published patents or applications. Through prediction and personal experience, the difficulty of synthesizing these 20 new structures was analyzed, and compound 0001 was chosen as our synthetic target, and a series of structures (**8a–l**) similar to compound 0001 were synthesized. Finally, the inhibitory activities of these compounds against bacteria *E. coli*, *P. aeruginosa*, *B. subtilis* and *S. aureus* were determined. The results showed that compound **8a–l** had obvious inhibitory activity against these four bacteria, which proved the accuracy of our compound generation model.

 Received 20th March 2022
 Accepted 26th July 2022

DOI: 10.1039/d2ra01807a

rsc.li/rsc-advances

1. Introduction

At present, bacterial infection¹ is still the main disease endangering human health, and the systemic and local application of antibiotics is the main way to kill pathogenic bacteria *in vivo*.² As the first choice for anti-trichomonas and anti-anaerobic bacteria, metronidazole is usually used in combination with other antibiotics in various clinical fields.³ As a typical representative of nitroimidazole drugs, metronidazole has more extensive clinical application because of its high curative effect, short course of treatment, long half-life and good tolerance.⁴ However, despite its wide clinical application, metronidazole still has a wide range of side effects. Researchers have conducted clinical trials on metronidazole in patients with oral

inflammation in many regions, and found that about 1/3 of patients have adverse reactions, mainly in the digestive tract and nervous system.⁵ Therefore, the development of metronidazole derivatives with new skeletons is still of great significance.⁶

The starting point of traditional ligand-based drug design methods, such as the 2D/3D Quantitative Structure–Activity Relationship (QSAR) and pharmacophore model,⁷ is based on the possible common structural basis between a series of ligands with similar structure, the same action type and different activity. Therefore, their common pharmacophores can be found on this structural basis, and new skeleton compounds can be found. The implementation steps of this method include calculating the descriptors of the collected compounds, such as molecular weight, logarithmic *p* value and hydrogen bond number, donor or recipient, and then creating quantitative models and physiological activity, toxicity and other effects as response values by using these descriptors as features. Although this method is very simple, its effectiveness and wide use must be remembered. It has an inherent limitation, that is, it depends on the interpretation ability of the calculated descriptor, which is directly related to the structure of the compounds in training set.⁸ Therefore, they may not be

^aSchool of Life Sciences and Medicine, Shandong University of Technology, Zibo, 255049 Shandong, China. E-mail: 295722387@qq.com; niuyzh12@lzu.edu.cn

^bInstitute of Modern Physics, Chinese Academy of Science, Lanzhou, 730000 Gansu, China

^cSchool of Physics and Technology, Lanzhou University, Lanzhou 730000, China

† Electronic supplementary information (ESI) available. See <https://doi.org/10.1039/d2ra01807a>

‡ These authors contributed equally to this work.



able to cover all the factor response values required to explain the problem. Moreover, this kind of method finally obtains the candidate compounds by screening the compound library.⁹

Recent developments in the field of Artificial Intelligence (AI) and big data¹⁰ show that it is possible to fundamentally change the accuracy and reliability of computational models, including drug discovery.^{11,12} The model generation method based on neural network has been widely used in drug design, such as affinity prediction, compatibility prediction, synthetic route design and protein folding prediction.^{13,14} Compared with QSAR and other calculation methods, the model shows superior performance in calculation speed and accuracy. In recent years, many deep-seated generative models have been proposed, including variational automatic encoder,¹⁵ generative game network¹⁶ and terminal RNN.¹⁷ They understood the basic data distribution in an unsupervised environment and explored the broad space of pharmaceutical chemistry by encoding molecules into a continuous potential space. The structure of compounds is usually encoded by a molecular input line input system (e.g. the Simplified Molecular-Input Line-Entry System, SMILES) or represented by molecular graphs, having sequence structures similar to natural languages. Therefore, machine learning algorithms (e.g. RNN) for natural language processing (e.g. text generation and machine translation) can be transplanted to the task of small molecule generation. The RNN generation model will simplify the molecular input line input system representation or molecular graph representation used to train the learning characteristics of deep neural network models. Memory enhanced RNN is introduced to improve the efficiency of generating effective molecules.¹⁸ RNN has been shown to be fine-tuned by Transfer Learning (TL) to produce molecules with structures similar to similar to drugs with known activity, which are known to be active for specific targets. Therefore, in order to design metronidazole compounds, we apply TL to this work, and combine the generation model with the prediction model to guide the generator to generate new chemical entities with metronidazole compounds.

In this work, we propose a method to redesign metronidazole derivatives using RNN deep learning method. Firstly, we train a gated recurrent unit (GRU)-based generative model to generate libraries of valid SMILES strings with high accuracy. Then we use transfer learning to fine-tune our model, generating molecules that are structurally similar to drugs with known activities. Even with just a few representative molecules for transfer learning training, our approach yielded structures with similar chemical characteristics to known scaffolds. Subsequently, the library activity of our pipeline design is verified. We performed cluster analysis on the structures of the new compounds and selected all small molecular compounds containing metronidazole structures in different categories. Of the 20 selected structures, 19 may not belong to the scope of any published patents or applications. Finally, we analyzed the synthesis difficulty of these 20 new structures through prediction and personal experience, selected compound 0001 as our synthesis target, and synthesized a series of similar structures (**8a–l**) of 0001. The antibacterial activity test shows that these compounds have obvious inhibitory effects on four kinds of

bacteria: *E. coli*, *P. aeruginosa*, *B. subtilis* and *S. aureus*, which proves the accuracy of our RNN production model.

2. Materials and methods

2.1 Deep learning algorithms

As with the text generation task, the first step in *de novo* drug design is to train a generator, which aims to learn rules of organic chemistry that define SMILES strings corresponding to realistic chemical structures.¹⁹ However, random generation without lead experience is too blind to be generated for specific tasks or targets.²⁰ Therefore, how to endow deep learning methods with specific research experience is the key to molecular design for specific tasks. In our work, deep learning algorithms were employed to generate molecules by a pre-trained generator model coupled with a transfer learning model introducing the existing leading experience (Fig. 1).

2.1.1 Generative model. Our generative model (Fig. 1) consists of an encoder, a decoder and a stack-augmented GRU. Different from other regular RNN model, stack-augmented GRU enhances the network's memory of previous information by delivering the dynamic memory stored in the stack to the calculation of the hidden layer at the next time step, which enabled the generation of chemically valid SMILES with high accuracy.^{19,21}

In our model, the dimension of the stack-augmented layer is 1500, and the depth is 200, which means that 200 steps of sequence information can be stored in stack memory. The GRU has 1500 + 1500 units for processing splicing vectors from hidden state and stack memory, and returns a 1500-dimensional vector containing the current token and previous sequence information, and finally returns the predicted probability distribution of the next token through the decoder. The parameters of the model are updated by reducing the cross-entropy loss between the real tokens and the predicted tokens. In the training process, the optimizer we used was AMSGrad, the learning rate was set as 0.0005, and the model tended to converge after 500 iterations of training. In our previous work, the performance of generative models with the above parameters was evaluated in terms of generating effective molecular proportions and generating molecular properties. We found that the 1-layer GRU performs comparable to the 4-layer GRU and can be successfully used for small molecule library design.²² Therefore, we use the above model to accelerate the development of antibacterial drugs, and the trained stack-augmented GRU is saved as a pretrained model to be weighted by a task-specific transfer learning model.

2.1.2 Transfer learning (TL). To introduce the existing leading experience of the specific targets, the GRU-based generative model was fine-tuned by transfer learning. Firstly, molecules with metronidazole rings from the ChEMBL database²³ and similar structures from the ChEMBL based on the active skeletons of metronidazole derivatives (including nitroimidazole derivatives) reported in the literature^{24–31} were collected, for a total of 580 small molecules as a training set for transfer learning. Then, transfer learning method was used to guide the generative model to learn those known active



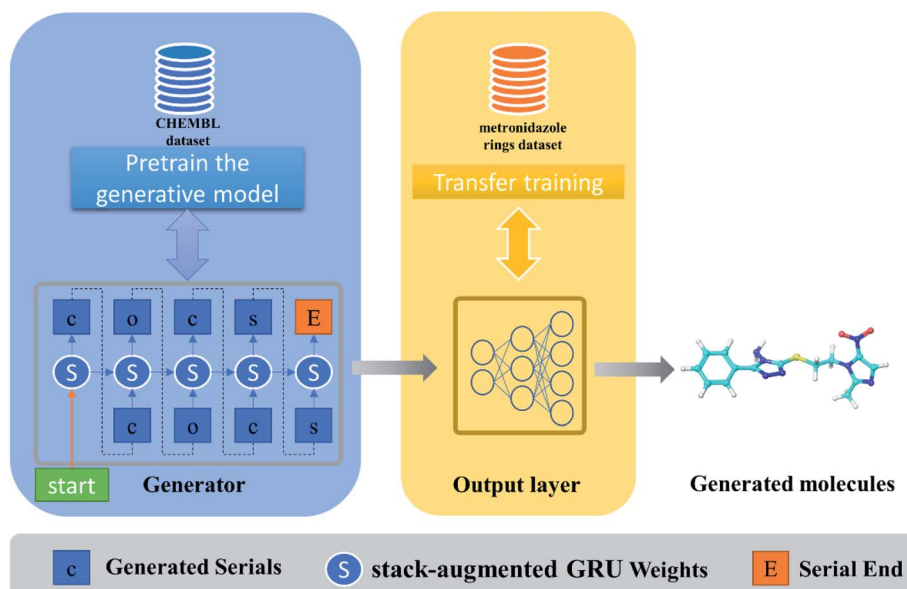


Fig. 1 Pipeline of generative model for novel compound generation.

fragments and generate a library of compounds starting from those active fragments.

During transfer learning, all the layers of the generative model were frozen, which will not be adjusted in the process of gradient calculation and backward transmission, except for the last decoder module. Only the parameters of the decoder layer are adjusted, which prevent the model forget the molecular features on small samples, so as to generate compounds that are similar to the training set. The weight of the pretrained model were loaded and trained on the small samples, until the training stopped when the sample distribution generated by the model was similar to the data of the training set but the repetition rate was low.

2.2 Cluster analysis and synthesis difficulty analysis of compounds

Cluster analysis of compounds was completed in the canvas of schrödinger2015,³² and the molecular fingerprint types were selected as hashed. Synthetic Accessibility Score (SAS)³³ is designed according to concise rules, which can quickly evaluate a large number of compounds. This method³⁴ is based on the “complexity” of molecules, but in order to combine the action of reagents and reactions, complex structures can be constructed immediately, so the assumption that “often occurring substructures are easy to synthesize” is used. The SAS is calculated according to the follow:

$$\text{SAS} = \text{fragmentScore} - \text{complexityPenalty} \quad (1)$$

“*FragmentScore*” is to capture “historical synthesis knowledge” by analyzing the common structural characteristics of a large number of synthesized molecules. The score is calculated as the sum of the contributions of all fragments in the molecule divided by the number of fragments in the molecule.

The database of contributions has been generated by statistical analysis of substructures in PubChem database³⁵ “ComplexityPenaltyonly” considers factors such as macrocycle and molecular weight. Standardize the value from 1 (simple) to 10 (difficult).

A measure of drug-likeness called weighted Quantitative Estimation of Drug-Likeness Molecules (QED_w)³⁶ was applied in our study.

$$\text{QED}_w = \exp \left(\frac{\sum_{i=1}^n w_i \ln d_i}{\sum_{i=1}^n w_i} \right) \quad (2)$$

It is calculated as shown in eqn (2), in which *d* represents the individual desirability functions (including molecular weight, log *P*, topological polar surface area, number of hydrogen bond donors and acceptors, number of aromatic rings and rotatable bonds, harmful chemical functional group distribution and *etc.*), *w* is the weight applied to each function and *n* is the number of descriptors. SAS and QED_w were calculated by the RDKit toolkit [<https://www.rdkit.org>].

2.3 Materials and measurements

All the starting materials, chemicals and solvents used in the synthesis of metronidazole derivatives were analytical reagent grade and purchased commercially from Aladdin Industrial Corporation (China). All reactions were routinely checked by Thin-Layer Chromatography (TLC) on 0.25 mm silica gel plates (silica GF 254). ¹H NMR spectra were carried out at ambient temperature on a Bruke AVANCE III 400 spectrometer using tetramethylsilane (TMS) as an internal standard. Mass spectra were measured with an Autoflex II TM instrument for ESI-MS. Elemental analyses were analyzed on a PerkinElmer model



2400 analyzer. The intermediate 4-amino-3-substituent-1,2,4-triazole-5-thiol (**5a–l**) was synthesized according to the literature method.³⁷

2.4 General method of synthesis of target compounds **8a–l**

Metronidazole (1.71 g, 10 mmol), 4-toluene sulfochloride (2.28 g, 12 mmol) and trimethylamine (TEA) (1.67 mL, 12 mmol) were dissolved in CH_2Cl_2 (15 mL). The reaction mixture was stirred at room temperature (298 K) overnight. After the completion of the reaction, as monitored by TLC, the resulted precipitate was filtered and washed with dilute hydrochloric acid and ethanol to obtain white crystal powder 2-(2-methyl-5-nitro-1*H*-imidazol-1-yl)ethyl 4-methylbenzenesulfonate (**6**). A solution of **6** (3.25 g, 10 mmol), sodium iodide (2.25 g, 15 mmol), and acetone (25 mL) was refluxed with stirring for 10 h. The reaction mixture was cooled and filtered, then the filtrate was evaporated under reduced pressure to afford 1-(2-iodoethyl)-2-methyl-5-nitro-1*H*-imidazole (**7**). **5** (5 mmol) and potassium hydroxide (0.28 g, 5 mmol) were dissolved in methanol (25 mL), stirred for 30 min at room temperature. Later, slowly added **7** (1.40 g, 5 mmol) to the reaction mixture, and heated to reflux for 5–8 h. The reaction progress was detected by using TLC technique. After completion of the reaction, the mixture was concentrated under reduced pressure to afford a crude solid. The acquired crude solid was purified by column chromatography skill eluting with dichloromethane and methanol to obtain pure metronidazole-triazole compounds **8a–l** (Fig. 4).

2.4.1 3-(2-Fluorophenyl)-5-((2-(2-methyl-5-nitro-1*H*-imidazol-1-yl)ethyl)thio)-1,2,4-triazol-4-amine (8a). White powder, 1.16 g, yield 64.1%. ^1H NMR (400 MHz, CDCl_3) δ : 2.62 (s, 3H, CH_3), 3.62 (t, 2H, CH_2), 4.76 (s, 2H, NH_2), 4.83 (t, 2H, CH_2), 7.24–7.28 (m, 1H, ArH), 7.35 (t, J = 8.0 Hz, 1H, ArH), 7.57 (q, 1H, ArH), 7.72 (t, 1H, ArH), 7.96 (s, 1H, MTZH). ESI-MS: 402.17 ($[\text{M} + \text{K}]^+$). Anal. calcd for $\text{C}_{14}\text{H}_{14}\text{FN}_7\text{O}_2\text{S}$: C, 46.28; H, 3.88; N, 26.98. Found: C, 46.45; H, 3.86; N, 27.07.

2.4.2 3-(3-Fluorophenyl)-5-((2-(2-methyl-5-nitro-1*H*-imidazol-1-yl)ethyl)thio)-1,2,4-triazol-4-amine (8b). White powder, 1.09 g, yield 60.5%. ^1H NMR (400 MHz, CDCl_3) δ : 2.62 (s, 3H, CH_3), 3.62 (t, 2H, CH_2), 4.75 (s, 2H, NH_2), 4.84 (t, 2H, CH_2), 7.21 (t, 1H, ArH), 7.45–7.51 (m, 1H, ArH), 7.82–7.87 (m, 2H, ArH), 7.97 (s, 1H, MTZH). ESI-MS: 402.25 ($[\text{M} + \text{K}]^+$). Anal. calcd for $\text{C}_{14}\text{H}_{14}\text{FN}_7\text{O}_2\text{S}$: C, 46.28; H, 3.88; N, 26.98. Found: C, 46.41; H, 3.85; N, 27.05.

2.4.3 3-(4-Fluorophenyl)-5-((2-(2-methyl-5-nitro-1*H*-imidazol-1-yl)ethyl)thio)-1,2,4-triazol-4-amine (8c). White powder, 1.18 g, yield 62.4%. ^1H NMR (400 MHz, CDCl_3) δ : 2.63 (s, 3H, CH_3), 3.62 (t, 2H, CH_2), 4.65 (s, 2H, NH_2), 4.84 (t, 2H, CH_2), 7.18–7.22 (m, 2H, ArH), 7.97 (s, 1H, MTZH), 8.04–8.07 (m, 2H, ArH). ESI-MS: 386.25 ($[\text{M} + \text{Na}]^+$). Anal. calcd for $\text{C}_{14}\text{H}_{14}\text{FN}_7\text{O}_2\text{S}$: C, 46.28; H, 3.88; N, 26.98. Found: C, 46.43; H, 3.85; N, 27.07.

2.4.4 3-(2-Chlorophenyl)-5-((2-(2-methyl-5-nitro-1*H*-imidazol-1-yl)ethyl)thio)-1,2,4-triazol-4-amine (8d). White powder, 1.17 g, yield 61.6%. ^1H NMR (400 MHz, CDCl_3) δ : 2.60 (s, 3H, CH_3), 3.63 (t, 2H, CH_2), 4.76 (s, 2H, NH_2), 4.84 (t, 2H,

CH_2), 7.43–7.47 (m, 1H, ArH), 7.49–7.55 (m, 2H, ArH), 7.58 (d, 1H, ArH), 7.96 (s, 1H, MTZH). ESI-MS: 402.25 ($[\text{M} + \text{Na}]^+$). Anal. calcd for $\text{C}_{14}\text{H}_{14}\text{ClN}_7\text{O}_2\text{S}$: C, 44.27; H, 3.72; N, 25.81. Found: C, 44.40; H, 3.71; N, 25.89.

2.4.5 3-(3-Chlorophenyl)-5-((2-(2-methyl-5-nitro-1*H*-imidazol-1-yl)ethyl)thio)-1,2,4-triazol-4-amine (8e). White powder, 1.21 g, yield 63.8%. ^1H NMR (400 MHz, CDCl_3) δ : 2.62 (s, 3H, CH_3), 3.62 (t, 2H, CH_2), 4.81 (s, 2H, NH_2), 4.83 (t, 2H, CH_2), 7.42–7.49 (m, 2H, ArH), 7.96–7.98 (m, 2H, ArH), 8.10 (s, 1H, MTZH). ESI-MS: 402.17 ($[\text{M} + \text{Na}]^+$). Anal. calcd for $\text{C}_{14}\text{H}_{14}\text{ClN}_7\text{O}_2\text{S}$: C, 44.27; H, 3.72; N, 25.81. Found: C, 44.41; H, 3.71; N, 25.86.

2.4.6 3-(4-Chlorophenyl)-5-((2-(2-methyl-5-nitro-1*H*-imidazol-1-yl)ethyl)thio)-1,2,4-triazol-4-amine (8f). White powder, 1.18 g, yield 62.4%. ^1H NMR (400 MHz, CDCl_3) δ : 2.62 (s, 3H, CH_3), 3.62 (t, 2H, CH_2), 4.70 (s, 2H, NH_2), 4.84 (t, 2H, CH_2), 7.47–7.49 (m, 2H, ArH), 7.97 (s, 1H, MTZH), 8.0–8.03 (m, 2H, ArH). ESI-MS: 402.17 ($[\text{M} + \text{Na}]^+$). Anal. calcd for $\text{C}_{14}\text{H}_{14}\text{ClN}_7\text{O}_2\text{S}$: C, 44.27; H, 3.72; N, 25.81. Found: C, 44.35; H, 3.70; N, 25.91.

2.4.7 3-(2-Tolyl)-5-((2-(2-methyl-5-nitro-1*H*-imidazol-1-yl)ethyl)thio)-1,2,4-triazol-4-amine (8g). White powder, 0.91 g, yield 50.8%. ^1H NMR (400 MHz, CDCl_3) δ : 2.34 (s, 3H, Ar-CH_3), 2.61 (s, 3H, CH_3), 3.62 (t, 2H, CH_2), 4.54 (s, 2H, NH_2), 4.84 (t, 2H, CH_2), 7.32 (t, 1H, ArH), 7.32 (d, 2H, ArH), 7.42–7.46 (m, 1H, ArH), 7.96 (s, 1H, MTZH). ESI-MS: 382.17 ($[\text{M} + \text{Na}]^+$). Anal. calcd for $\text{C}_{15}\text{H}_{17}\text{N}_7\text{O}_2\text{S}$: C, 50.13; H, 4.77; N, 27.28. Found: C, 50.27; H, 4.75; N, 27.36.

2.4.8 3-(3-Tolyl)-5-((2-(2-methyl-5-nitro-1*H*-imidazol-1-yl)ethyl)thio)-1,2,4-triazol-4-amine (8h). White powder, 1.05 g, yield 58.4%. ^1H NMR (400 MHz, CDCl_3) δ : 2.43 (s, 3H, Ar-CH_3), 2.61 (s, 3H, CH_3), 3.62 (t, 2H, CH_2), 4.76 (s, 2H, NH_2), 4.82 (t, 2H, CH_2), 7.32 (d, 1H, ArH), 7.39 (t, 1H, ArH), 7.74 (t, 2H, ArH), 7.95 (s, 1H, MTZH). ESI-MS: 382.25 ($[\text{M} + \text{Na}]^+$). Anal. calcd for $\text{C}_{15}\text{H}_{17}\text{N}_7\text{O}_2\text{S}$: C, 50.13; H, 4.77; N, 27.28. Found: C, 50.28; H, 4.75; N, 27.38.

2.4.9 3-(4-Tolyl)-5-((2-(2-methyl-5-nitro-1*H*-imidazol-1-yl)ethyl)thio)-1,2,4-triazol-4-amine (8i). White powder, 1.02 g, yield 56.6%. ^1H NMR (400 MHz, CDCl_3) δ : 2.38 (s, 3H, Ar-CH_3), 2.49 (s, 3H, CH_3), 3.45 (s, 2H, CH_2), 3.59 (s, 2H, CH_2), 4.70 (s, 2H, NH_2), 6.16 (d, 2H, ArH), 7.39 (t, 1H, ArH), 7.90 (d, 2H, ArH), 8.02 (s, 1H, MTZH). ESI-MS: 382.42 ($[\text{M} + \text{Na}]^+$). Anal. calcd for $\text{C}_{15}\text{H}_{17}\text{N}_7\text{O}_2\text{S}$: C, 50.13; H, 4.77; N, 27.28. Found: C, 50.32; H, 4.74; N, 27.42.

2.4.10 3-(Pyridin-2-yl)-5-((2-(2-methyl-5-nitro-1*H*-imidazol-1-yl)ethyl)thio)-1,2,4-triazol-4-amine (8j). White powder, 1.08 g, yield 61.7%. ^1H NMR (400 MHz, CDCl_3) δ : 2.61 (s, 3H, CH_3), 3.63 (t, 2H, CH_2), 4.82 (t, 2H, CH_2), 6.08 (s, 2H, NH_2), 7.38–7.42 (m, 1H, ArH), 7.86–7.90 (m, 1H, ArH), 7.96 (s, 1H, MTZH), 8.27 (d, 1H, ArH), 8.63 (d, 1H, ArH). ESI-MS: 369.17 ($[\text{M} + \text{Na}]^+$). Anal. calcd for $\text{C}_{13}\text{H}_{14}\text{N}_8\text{O}_2\text{S}$: C, 45.08; H, 4.07; N, 32.35. Found: C, 45.21; H, 4.05; N, 32.44.

2.4.11 3-(Pyridin-3-yl)-5-((2-(2-methyl-5-nitro-1*H*-imidazol-1-yl)ethyl)thio)-1,2,4-triazol-4-amine (8k). White powder, 1.10 g, yield 63.4%. ^1H NMR (400 MHz, DMSO) δ : 2.48 (s, 3H, CH_3), 3.60 (t, 2H, CH_2), 4.70 (t, 2H, CH_2), 6.22 (s, 2H, NH_2), 7.52 (d, 1H, ArH), 7.59 (dd, 1H, ArH), 8.03 (s, 1H, MTZH), 8.35–8.38 (m, 1H, ArH), 8.70 (dd, 1H, ArH). ESI-MS: 368.33 ($[\text{M} + \text{Na}]^+$). Anal. calcd



for $C_{13}H_{14}N_8O_2S$: C, 45.08; H, 4.07; N, 32.35. Found: C, 45.26; H, 4.05; N, 32.48.

2.4.12 3-(Pyridin-4-yl)-5-((2-(2-methyl-5-nitro-1H-imidazol-1-yl)ethyl)thio)-1,2,4-triazol-4-amine (8l). White powder, 1.05 g, yield 60.9%. 1H NMR (400 MHz, DMSO) δ : 2.47 (s, 3H, CH_3), 3.61 (t, 2H, CH_2), 4.70 (t, 2H, CH_2), 6.27 (s, 2H, NH_2), 7.99–8.06 (m, 3H, ArH), 8.73 (s, 1H, ArH), 8.75 (s, 1H, MTZH). ESI-MS: 369.33 ($[M + Na]^+$). Anal. calcd for $C_{13}H_{14}N_8O_2S$: C, 45.08; H, 4.07; N, 32.35. Found: C, 45.17; H, 4.04; N, 32.45.

2.5 Bioassay conditions

The antibacterial activity of the synthesized compounds was evaluated against two Gram-negative bacterial strains, *Escherichia coli* ATCC 35218 and *Pseudomonas aeruginosa* ATCC 27853, and two Gram-positive bacterial strains, *Bacillus subtilis* ATCC 6633 and *Staphylococcus aureus* ATCC 6538. The bioassay was conducted using MH medium (Mueller–Hinton medium: casein hydrolysate 17.5 g, soluble starch 1.5 g, beef extract 1000 mL). The IC_{50} (half minimum inhibitory concentrations) of the test compounds were determined by a colorimetric method using the dye MTT (3-(4,5-dimethylthiazol-2-yl)-2,5-diphenyl tetrazoliumbromide). Clinically used antibiotics streptomycin was used as reference. The antibacterial activities were evaluated by the method reported before. The procedure of antimicrobial activity was given in detail in the ESI 1.†

3. Results and discussion

3.1 Deep learning model accuracy evaluation

To train the generative model, we collected \sim 1.6 million small molecules from CHEMBL,³⁸ and each small molecule is represented as SMILES format to train a generator of Seq2Seq. The SMILES dataset was preprocessed by applying sequential filters to remove stereochemistry, salts, and molecules with undesirable atoms (metal atoms) or groups.²⁰ In the end, \sim 1.6 million small molecules with a length of 100 or less were retained for

training the generative model. In order to evaluate the accuracy of the pretrained generator in generating chemically valid molecules, a total of 100 000 compounds were sampled from the generation model for 10 times, 10 000 compounds at a time, and an average of 95.6% of the small molecules in all sample batches were chemically valid (removal of redundant and can be parsed by the RDKit library). We predicted the QED and SAS of all the compounds produced by the GRU-based model with existing metronidazole compounds, and the results show that the molecules generated by GRU-based generators have higher drug-likeness properties and lower synthesizable scores (Fig. 2).

3.2 Discovery of new metronidazole derivative

After TL, the RNN model generated 3314 small molecular compounds (ESI 2†), of which 321 compounds containing the metronidazole groups were retained, and they were input into canvas to calculate the binary fingerprints of all small molecules. Then hierarchical clustering was carried out based on the tanimoto similarity metric. The 321 compounds are grouped into 20 categories by default, while the merging distance is 0.8, and the representative structure with the lowest SAS are selected from each category shown in Fig. 3.

No matter how to obtain lead compounds, it is very important to evaluate the synthesis difficulty of candidate lead compounds, and it is a priority issue. In any case, “easy synthesis” of compounds must be considered at a certain stage of research. In this case, if other indexes (such as activity) are given priority and “difficulty of synthesis” is considered at the end, compounds with similar chemical types and skeletons tend to be selected. We evaluated the SAS of 20 selected compounds by RDKit, and the results are shown in Fig. 3. Molecules with the high SAS are difficult to synthesize, whereas, molecules with the low SAS values are easily synthetically accessible. Because the lowest SAS are 0355 (SAS: 2.50), 0001 and 0799 (SAS: 2.56) among the 20 compounds, the three compounds are the easiest to synthesize theoretically. However,

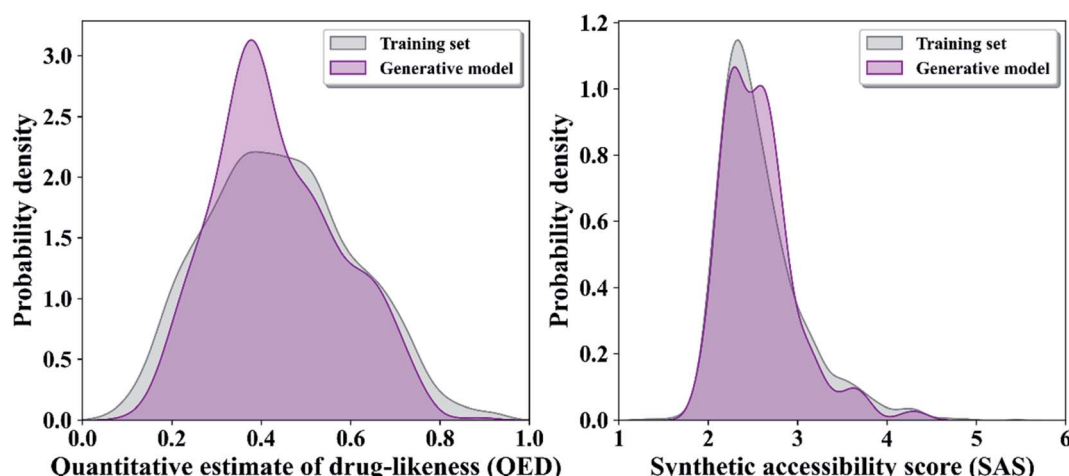


Fig. 2 Distribution of the quantitative estimate of drug-likeness scores (QED) (A) and distribution of the synthetic accessibility scores (SAS) in two generator and existing metronidazole compounds.



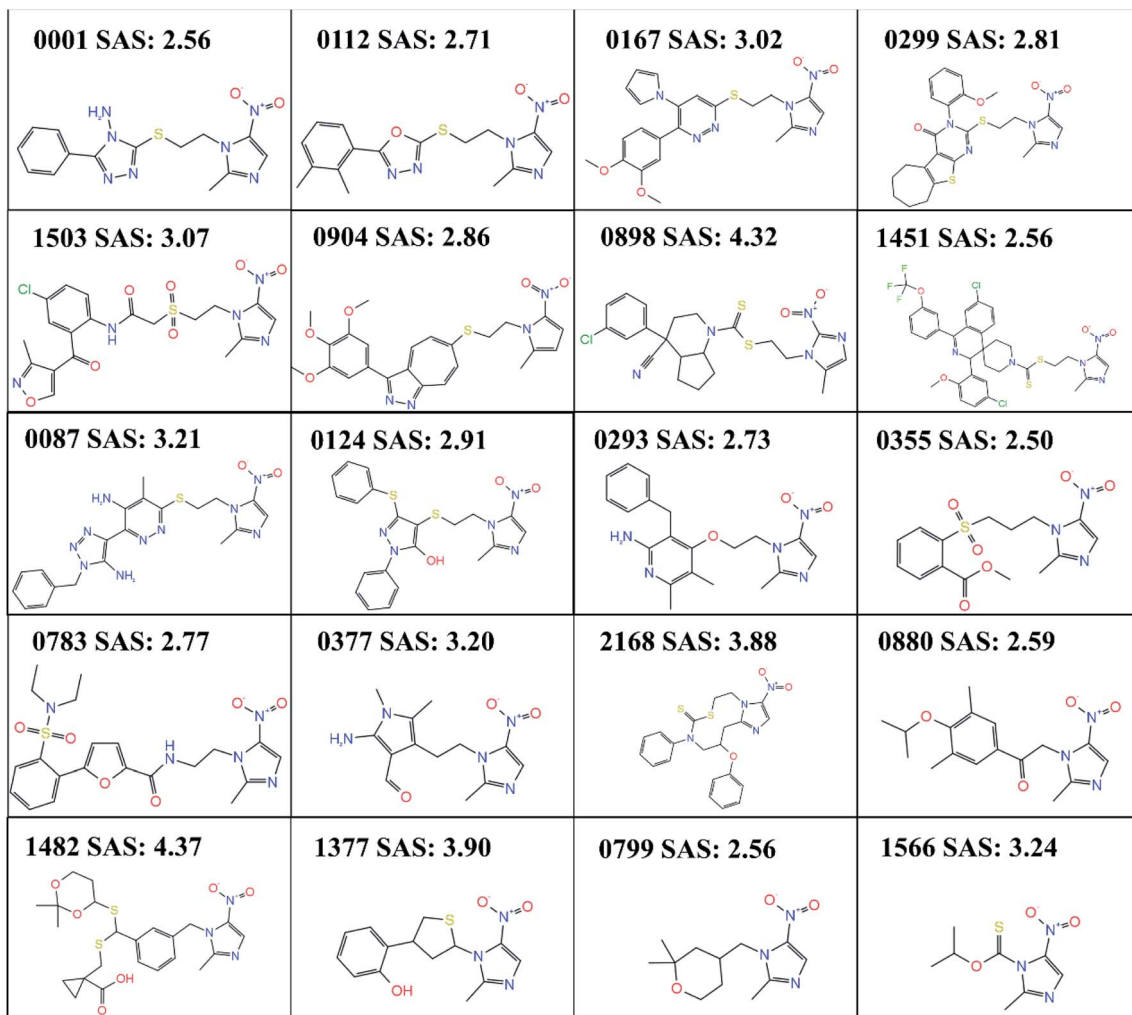


Fig. 3 20 compounds with different skeleton obtained by clustering. SAS refers to the synthetic accessibility scores.

the software prediction is inevitably mechanical. We also predicted the synthetic route of 0355 and 0799 by using chemical.ai (<https://chemical.ai/>), as shown in Fig. S1.† For compound 0799, we need to consider the following points when considering the optimization of synthetic route: (1) Raw materials like (2) or (4) are expensive; (2) the compound 0799 has chiral carbon atoms, and it needs to be resolved during the synthesis process, which increases the complexity of the synthesis; (3) it is difficult to obtain high purity of compounds containing cyclic ether structure during purification; however, for compound 0355, its raw materials (6)–(9) can't be purchased directly. As mentioned above, we have more experience in the synthesis of 0001, so we tried to synthesize 0001 firstly. Furthermore, compounds 0001 and 0112 are highly similar in structure, while 0112 has been reported to have obvious antibacterial activity. At the same time, we also found that there are many structures with methyl or chlorine atoms substituted on the benzene ring of 0001 among the 3314 small molecular structures we generated, such as 0004 and 0041. Therefore, we first synthesized 0001 and measured its antibacterial activity,

and then continued to try to synthesize 11 other compounds with substituents on the benzene ring of 0001 and measured their antibacterial activity.

3.3 Synthesis of candidate compounds

The synthetic route of target compounds 0001 and its similar structures (**8a–l**) was showed in Fig. 4. To obtain the designed metronidazole-triazole derivatives, we began with the esterification reaction of aromatic acids (**1**) in methanol, which resulted in aromatic esters (**2**) followed by reaction with hydrazine hydrate to get hydrazide derivatives (**3**). 1,2,4-Triazole derivatives (**5**) were acquired by first nucleophilic addition reaction of **3** and carbon disulfide to obtain (**4**), followed by condensation reaction with hydrazine hydrate. 1-(2-Iodoethyl)-2-methyl-5-nitro-1*H*-imidazole (**7**) was obtained by two successive substitution reaction of metronidazole. Finally, nucleophilic substitution reaction between (**7**) and (**5**) in the presence of potassium hydroxide yielded **8a–l**. The synthesized analogs were characterized by utilizing ESI-MS and ¹H-NMR spectroscopic techniques (Fig. S2–25 in ESI 1†).



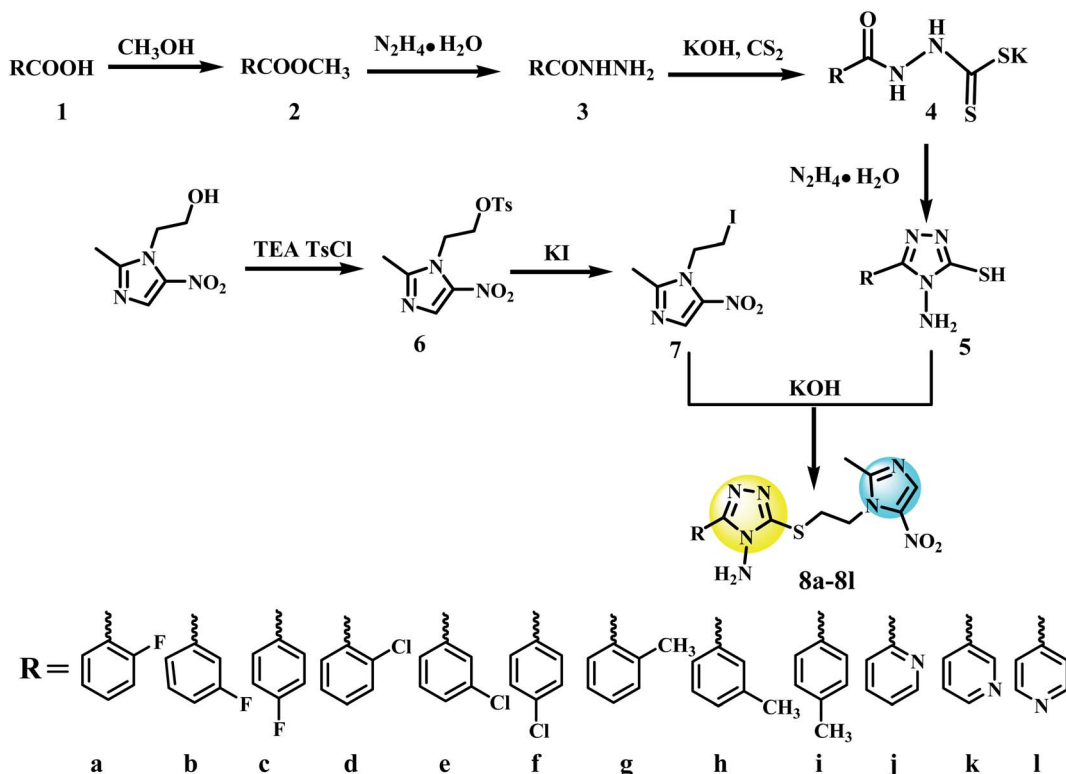


Fig. 4 Synthesis process of compound 8a–l.

3.4 In vitro antibacterial activity

The antibacterial activity of the synthesized metronidazole derivatives **8a–l** was tested using the 3-(4,5-dimethylthiazol-2-yl)-2,5-diphenyltetrazolium bromide (MTT) method. The results of IC_{50} are presented in Table 1. Known antibiotic like streptomycin was used as control drug. As our results show, the tested compounds exhibited various degrees of inhibition against Gram-positive and Gram-negative bacteria. And against the all tested bacteria, metronidazole derivatives **8a–l** showed higher antibacterial activity against Gram positive strains, with IC_{50} values ranging from 7.61 to 18.39 $\mu\text{g mL}^{-1}$ for *B. subtilis*, and 2.46 to 13.49 $\mu\text{g mL}^{-1}$ for *S. aureus*, respectively. *S. aureus* was observed to be the most sensitive bacteria, compound **8i** with *p*-methylphenyl group on the 1,2,4-triazole skeleton showed the best antibacterial activity against *S. aureus*. Compared to the reference drug streptomycin, **8a–l** had less potency against Gram negative strains, only compounds **8g**, **8h** and **8i**, with methylphenyl group on the 1,2,4-triazole skeleton had comparable efficacy against *P. aeruginosa* with IC_{50} values ranging from 5.74 to 6.71 $\mu\text{g mL}^{-1}$. Regarding the effect of the substituent on the phenyl moiety of the 1,2,4-triazole skeleton, the substitution with electron-donating methyl group had a better antibacterial activity towards both Gram-positive and Gram-negative bacteria, compared with electron-withdrawing halogen groups at the same position. Moreover, structure-activity relationship studies revealed the substituent at different positions led to different activity, and the potency order was *para* > *meta* > *ortho*.

Table 1 Inhibitory activity (IC_{50}) of compound **8a–l** against four kinds of bacteria

Compound	IC_{50} ($\mu\text{M L}^{-1}$)			
	<i>E. coli</i>	<i>P. aeruginosa</i>	<i>B. subtilis</i>	<i>S. aureus</i>
8a	72.64	99.52	45.65	28.21
8b	70.11	78.07	37.71	37.16
8c	61.46	69.61	29.15	20.8
8d	74.01	42.82	33.43	24.59
8e	60.63	49.95	37.92	19.97
8f	51.03	40.29	33.91	16.73
8g	59.11	15.99	26.02	11.98
8h	48.89	16.32	21.20	9.89
8i	42.51	18.69	18.97	6.85
8j	30.00	28.38	37.80	23.73
8k	38.64	37.51	53.15	25.90
8l	41.07	53.12	48.35	22.23
Streptomycin	22.92	12.48	16.22	8.67

4. Conclusions

Ligand-based *de novo* drug design method has benefited from the development in the machine learning community as applied to natural language processing and machine translation. RNN-based generation model is widely used, and transfer learning is used to further optimize the structure of compounds in order to produce molecules with desired



Table 2 Abbreviations

Abbreviations	Explanations
GRU	Gated recurrent unit
SMILES	Simplified molecular-input line-entry system
QSAR	Quantitative structure–activity relationship
AI	Artificial intelligence
TL	Transfer learning
RNN	Recurrent neural network
MTT	3-(4,5-Dimethylthiazol-2-yl)-2,5-diphenyltetrazolium bromide
SAS	Synthetic accessibility score
QED_w	Weighted quantitative estimation of drug-likeness
$\log P$	Oil–water partition coefficient
TLC	Thin-layer chromatography
TMS	Tetramethylsilane

properties. In this work, a series of metronidazole compounds were found by combining RNN neural network generation compound model, transfer learning and chemical synthesis. Collecting ~1.6 million small molecules from ChEMBL were used to train the generative stack-augmented GRU model. We then use transfer learning to fine-tune our model, generating molecules that are structurally similar to drugs with known activities. Even with just a few representative molecules for transfer learning training, our approach yielded structures with similar chemical characteristics to known scaffolds. Subsequently, the library activity of our pipeline design is verified. We performed cluster analysis on the structures of the new compounds and selected all small molecular compounds containing metronidazole structures in different categories. Of the 20 selected structures, 19 may not belong to the scope of any published patents or applications. Finally, we analyzed the synthesis difficulty of these 20 new structures through prediction and personal experience, selected compound 0001 as our synthesis target, and synthesized a series of similar structures (**8a–l**) of 0001. The inhibitory activities of these compounds on four bacteria *E. coli*, *P. aeruginosa*, *B. subtilis* and *S. aureus* were determined. The results showed that compound **8a–l** had obvious inhibitory activities on these four bacteria, which proved the accuracy of our compound generation model.

Appendix

Abbreviations are listed in Table 2.

Conflicts of interest

The authors declare that there is no conflict of interest in this work.

Acknowledgements

This work was supported by the Natural Foundation of Shandong Province (Grant No. ZR2018BB055).

References

- 1 M. M. Biernat and T. Wróbel, *Int. J. Mol. Sci.*, 2021, **22**.
- 2 F. Tao, S. Ma, H. Tao, L. Jin, Y. Luo, J. Zheng, W. Xiang and H. Deng, *Carbohydr. Polym.*, 2021, **251**, 117063.
- 3 D. L. Bourque, A. Neumayr, M. Libman and L. H. Chen, *J. Trav. Med.*, 2022, **29**, taab120.
- 4 Y. Nishikawa, N. Sato, S. Tsukinaga, K. Uchiyama, S. Koido, D. Ishikawa and T. Ohkusa, *Ther. Adv. Chronic Dis.*, 2021, **12**, 20406223211028790.
- 5 D. Cicek, B. Kandi, S. Bakar and D. Turgut, *J. Dermatol. Treat.*, 2009, **20**, 344–349.
- 6 O. P. S. Patel, O. J. Jesumoroti, L. J. Legoabe and R. M. Beteck, *Eur. J. Med. Chem.*, 2021, **210**, 112994.
- 7 I. Jabeen, P. Wetwitayaklung, P. Chiba, M. Pastor and G. F. Ecker, *J. Comput. Aided Mol. Des.*, 2013, **27**, 161–171.
- 8 R. Zanni, M. Galvez-Llompart, R. Garcia-Domenech and J. Galvez, *Expert Opin. Drug Discov.*, 2020, **15**, 1133–1144.
- 9 P. Li, Y. Niu, S. Li, X. Zu, M. Xiao, L. Yin, J. Feng, J. He and Y. Shen, *Chem. Biol. Drug Des.*, 2022, **99**, 222–232.
- 10 Z. Dlamini, F. Z. Frances, R. Hull and R. Marima, *Comput. Struct. Biotechnol. J.*, 2020, **18**, 2300–2311.
- 11 G. Hessler and K. H. Baringhaus, *Molecules*, 2018, **23**, 2520.
- 12 M. Thomas, A. Boardman, M. Garcia-Ortegon, H. Yang, C. de Graaf and A. Bender, *Methods Mol. Biol.*, 2022, **2390**, 1–59.
- 13 H. Öztürk, A. Özgür and E. Ozkirimli, *Bioinformatics*, 2018, **34**, i821–i829.
- 14 M. Eisenstein, *Nature*, 2021, **599**, 706–708.
- 15 Y. Deng, A. Sander, L. Faulstich and K. Denecke, *Artif. Intell. Med.*, 2019, **93**, 29–42.
- 16 G. Gao, J. Cao, Z. Bu, H.-j. Li and Z. Wu, *Expert Syst. Appl.*, 2018, **96**, 450–461.
- 17 J. Fei and Z. Wang, *IEEE Access*, 2020, **8**, 167965–167974.
- 18 Y. Yu, X. Si, C. Hu and J. Zhang, *Neural Comput.*, 2019, **31**, 1235–1270.
- 19 M. Popova, O. Isayev and A. Tropsha, *Sci. Adv.*, 2018, **4**, eaap7885.
- 20 S. R. Krishnan, N. Bung, G. Bulusu and A. Roy, *J. Chem. Inf. Model.*, 2021, **61**.
- 21 A. Joulin and T. Mikolov, *presented in part at the Proceedings of the 28th International Conference on Neural Information Processing Systems - Volume 1*, Montreal, Canada, 2015.
- 22 L. Yang, G. Yang, Z. Bing, Y. Tian, Y. Niu, L. Huang and L. Yang, *ACS Omega*, 2021, **6**, 33864–33873.
- 23 A. Gaulton, L. J. Bellis, A. P. Bento, J. Chambers, M. Davies, A. Hersey, Y. Light, S. McGlinchey, D. Michalovich, B. Al-Lazikani and J. P. Overington, *Nucleic Acids Res.*, 2012, **40**, D1100–D1107.
- 24 W.-J. Mao, P.-C. Lv, L. Shi, H.-Q. Li and H.-L. Zhu, *Bioorg. Med. Chem.*, 2009, **17**, 7531–7536.
- 25 Y. Luo, Y. Li, K.-M. Qiu, X. Lu, J. Fu and H.-L. Zhu, *Bioorg. Med. Chem.*, 2011, **19**, 6069–6076.
- 26 Y. Qian, H. J. Zhang, Z. Hao, X. Chen, J. Zhao and H. L. Zhu, *Bioorg. Med. Chem.*, 2010, **18**, 4991–4996.
- 27 S. F. Wang, Y. Wang, F. Yin, X. Qiao, S. Wu and L. Zhang, *Bioorg. Med. Chem.*, 2014, **22**, 2409–2415.



28 Z. H. Guo, Y. Yin, C. Wang, P. F. Wang, X. T. Zhang, Z. C. Wang and H. L. Zhu, *Bioorg. Med. Chem.*, 2015, **23**, 6148–6156.

29 Y. J. Qin, P. F. Wang, J. A. Makawana, Z. C. Wang, Z. N. Wang, Y. Gu, A. Q. Jiang and H. L. Zhu, *Bioorg. Med. Chem. Lett.*, 2014, **24**, 5279–5283.

30 L. Yao, Y. Luo, H. Yang, D. D. Zhu, S. Zhang, Z. J. Liu, H. B. Gong and H. L. Zhu, *Bioorg. Med. Chem.*, 2012, **20**, 4316–4322.

31 H. J. Zhang, D. D. Zhu, Z. L. Li, J. Sun and H. L. Zhu, *Eur. J. Med. Chem.*, 2011, **19**, 4513–4519.

32 H. Alogheli, G. Olanders, W. Schaal, P. Brandt and A. Karlén, *J. Chem. Inf. Model.*, 2017, **57**, 190–202.

33 J. C. Baber and M. Feher, *Mini Rev. Med. Chem.*, 2004, **4**, 681–692.

34 P. Ertl and A. Schuffenhauer, *J. Cheminf.*, 2009, **1**, 8.

35 S. Kim, J. Chen, T. Cheng, A. Gindulyte, J. He, S. He, Q. Li, B. A. Shoemaker, P. A. Thiessen, B. Yu, L. Zaslavsky, J. Zhang and E. E. Bolton, *Nucleic Acids Res.*, 2021, **49**, D1388–d1395.

36 G. R. Bickerton, G. V. Paolini, J. Besnard, S. Muresan and A. L. Hopkins, *Nat. Chem.*, 2012, **4**, 90–98.

37 Y.-P. Xu, Y.-H. Chen, Z.-J. Chen, J. Qin, S.-S. Qian and H.-L. Zhu, *Eur. J. Inorg. Chem.*, 2015, **2015**, 2076–2084.

38 G. Anna, H. Anne, N. Michał, B. Patrícia, C. Jon, M. David, M. Prudence, A. Francis, L. J. Bellis and C. U. Elena, *Nucleic Acids Res.*, 2017, D945–D954.

